Journal of Robotics, Networking and Artificial Life
Vol. 11(3); March (2026), pp. 247-253
ISSN (Online): 2352-6386; ISSN (Print): 2405-9021
https://alife-robotics.org/jrnal.html

Research Article

Design Principle and Analysis of an Output Cam for a Rotary Actuator Capable of Multidirectional Rapid Motion and Variable Stiffness

Katsuaki Suzuki[1]*, Yuya Nishida[2], Kenji Kimura[3], Kazuo Ishii[4]
[1]*Kumamoto Industrial Research Institute, 3-11-38 Higashi machi, Higashi-ku, Kumamoto 862-0901, Japan*
[2]*Kyushu Institute of Technology, 2-4 Hibikino, Wakamatsu-ku, Kitakyushu 808-0196, Fukuoka, Japan*
[3]*Department of Control Engineering, National Institute of Technology, Matsue College, 14-4 Nishi-ikuma-cho, Matsue-shi, Shimane, 690-8518, Japan*
[4]*Kyushu Institute of Technology, 2-4 Hibikino, Wakamatsu-ku, Kitakyushu 808-0196, Fukuoka, Japan*
Email: k-suzuki@kumamoto-iri.jp, y-nishida@lsse.kyutech.ac.jp, k-kimura@matsue-ct.ac.jp, ishii@brain.kyutech.ac.jp
*Corresponding Author

ARTICLE INFO

Article History

Received 25 November 2024
Accepted 03 March 2026

Keywords

Rapid motion
Variable stiffness
Cam mechanism

ABSTRACT

Production processes such as high-mix, low-volume manufacturing, where product specifications and task conditions change frequently, require mechanisms that can flexibly switch functions and offer high adaptability. However, achieving multifunctionality by simply combining multiple actuators increases cost, control-system complexity, and mass. To address these issues, this study proposes a novel rotary actuator that achieves normal motion, rapid motion, and variable stiffness with direction-independent output characteristics, using only two motors in combination with mechanical elements such as cam mechanisms and a differential mechanism. This paper describes the structure and functions of the proposed mechanism, the design principles of the output cam that governs the output characteristics, and a mathematical model of its rapid motion. Furthermore, computer-aided engineering simulations using the designed output cam are conducted to evaluate the output characteristics in the variable-stiffness mode and to compare the simulated rapid motion with the mathematical model, thereby validating the theoretical model.

1. Introduction

According to a report by the Organisation for Economic Co-operation and Development (OECD), the working-age population in many OECD member countries is expected to decline over the next few decades [1]. By 2060, the total working-age population across the OECD is projected to shrink by 8%, with more than one quarter of the member countries anticipating decreases of over 30% [1]. Furthermore, approximately 8.6 million manufacturing jobs were lost in OECD countries between 2000 and 2018 [2]. Amid these intensifying constraints on labor supply, the need for automation in manufacturing sites has grown, leading to increased use of robots for automation. In addition to the deployment of industrial robots, collaborative robots that can operate in the same workspace as humans are becoming widespread, and the collaborative robot market is projected to grow at an average annual rate of approximately 34–35% in the coming years [3]. However, in processes such as high-mix, low-volume production, where product specifications and operating conditions change frequently, the shapes of target objects and the lot sizes differ greatly from job to job, making it difficult to generalize automation methods and leaving many tasks still unautomated. Therefore, there is a strong demand for highly adaptable and versatile robotic mechanisms that can flexibly switch functions in accordance with changes in the task. In other words, “multifunctionality”—whereby a single device or joint structure can realize multiple modes of operation—has become a key requirement.

Among the various aspects of multifunctionality, the ability to combine compliance with high output is particularly important. By varying stiffness according to the contact state with the object and generating high output at the required moment, a single robot can handle tasks ranging from delicate manipulation to high-speed assembly and machining. To achieve this, joint structures that can actively switch their output characteristics at the mechanism level are required.

In typical robot joints, the output shaft is directly driven by an actuator through a reduction gear (normal motion). While this configuration offers simple control and high positioning accuracy, it is difficult to achieve both compliance and high output because the performance is

constrained by the motor output. For tasks such as high-speed grasping, impact inspection, and impact forming, where a large instantaneous output is required, “rapid motion” has been investigated, in which an actuator stores energy in an elastic element and drives the output shaft by releasing this stored energy [4–5]. Conversely, for tasks that require responsiveness to external forces, such as contour-following motion, manipulation of deformable objects, and impact absorption, “variable stiffness mechanisms,” which vary stiffness in response to external forces, are effective. These mechanisms mechanically adjust stiffness using nonlinear springs, antagonistic structures, and similar means, thereby compensating for control delays and realizing high-bandwidth force response [6–8]. However, many conventional mechanisms have been studied with a focus on a single function, and it is difficult to realize the three functions of normal motion, rapid motion, and variable stiffness with a single output shaft. Most existing multifunctional actuators that provide these capabilities are constructed by combining multiple actuators and clutches [9-10]. In contrast, this study proposes a mechanism that integrates all three functions using only two motors and mechanical elements.

The authors have previously proposed a mechanism that realizes normal motion, rapid motion triggered by latch release, and continuous variable stiffness by combining two motors with a cam mechanism, an antagonistic link mechanism, and compression springs [11–12]. However, in that mechanism, the output characteristics varied depending on the output shaft angle. To address this issue, we propose a new rotary actuator mechanism [13] composed of two motors and mechanical elements such as two types of cam mechanisms, a differential mechanism, and torsion springs. The key feature of the proposed mechanism is that a single output shaft exhibits identical output characteristics in all directions while simultaneously realizing the three functions of normal motion, rapid motion, and variable stiffness. Furthermore, by implementing all kinematic pairs solely as revolute joints, sliding losses are reduced and efficient energy transmission during rapid motion is achieved. This paper presents the structure and functions of the proposed mechanism and describes the design methodology and analysis results of the output cam mechanism responsible for rapid-motion and variable-stiffness operation.

2. Structure and Functions of the Proposed Mechanism

The conceptual model of the proposed mechanism is shown in Fig. 1. It consists of a pulley-equipped output shaft, two input pulleys, two sets of output cam mechanisms, two torsion springs, two sets of spring-compression cam mechanisms, two dry bearings, two one-way bearings, two sets of bevel-gear mechanisms, two motors, two sets of worm-gear mechanisms, two input spur gears, and one fixed spur gear.

Table 1 summarizes the driving patterns of the proposed mechanism and how they correspond to each function. In the normal-motion mode, motors L and R rotate in the same direction, causing the two input spur gears to rotate in the same direction via the worm-gear mechanisms. As a result, the housing rotates relative to the fixed spur gear, and the output shaft is driven in accordance with the motor outputs. In the variable-stiffness mode, motors L and R rotate in opposite directions, driving the two spring-compression cams via the bevel gears. This adjusts the compression of the springs and enables mechanical control of the stiffness at the output shaft. When both motors are at a standstill and a disturbance torque is applied to the output shaft, the output shaft and output cams are backdriven relative to the housing, exhibiting a characteristic in which the reaction torque increases with displacement. Rapid motion is initiated from a state in which both springs are compressed. First, one of the spring-compression cams is rotated, causing the corresponding cam follower to drop instantaneously from a notched section. Consequently, one of the two springs (the leading spring) is released first, and only the rocker arm in contact with that cam rotates under the force of the leading spring. This motion disturbs the internal force balance of the mechanism, and the torque stored in the other spring (the output-driving spring) is transmitted to the output shaft via the output cam mechanism, causing the output link to start rotating rapidly. Reversing the rotation directions of motors L and R results in rapid motion in the opposite rotational direction in the same manner. Owing to this differential principle, the mechanism has the potential to integrate the three functions of normal motion, rapid motion, and variable stiffness while maintaining identical output characteristics in all directions, even when the posture of the housing changes.

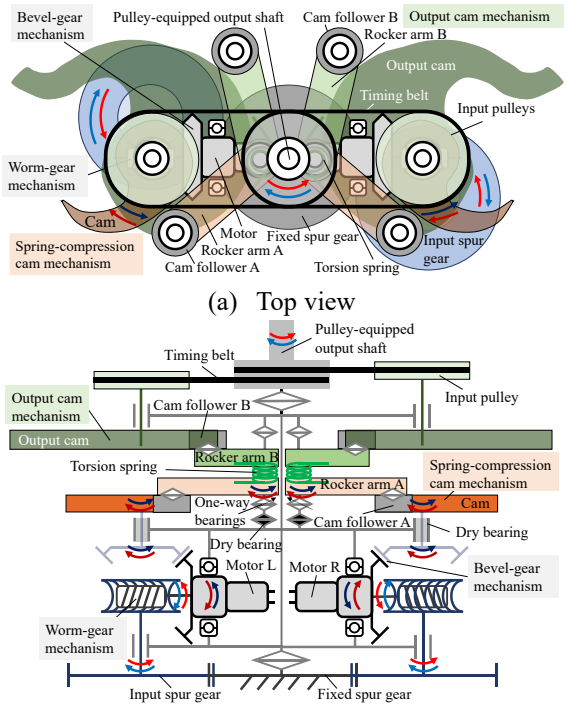

(a) Top view

(b) Front view

Fig.1 Rotary actuator

Table 1 Drive patterns and functions

State	Motor L	Motor R	Torsion Spring	Output Shaft
Normal motion Low Stiffness			Natural position	
Normal motion High Stiffness			Compressed	
Compression Adjustment			Compression / Extension	Stop
Rapid motion Spring release		Stop	Rapid Extension	
	Stop			
Disturbance acts Low Stiffness	Stop	Stop	Natural position	
Disturbance acts Low Stiffness	Stop	Stop	Compressed	

3. Design Principle of the Output Cam

This section describes the design concept and methodology of the output cam, which are the key elements determining the output characteristics in the rapid-motion and variable-stiffness modes of the proposed mechanism. A conceptual model of the output cam is shown in Fig. 2. The proposed mechanism adopts a structure in which the contour of the output cam directly realizes mechanical variable stiffness. Thus, when designing the output cam, priority was first given to achieving variable stiffness, and the realization of rapid motion was then taken into account. To realize variable stiffness, a nonlinear spring characteristic is constructed by combining a linear torsion spring with the cam. When the cam is backdriven in the direction that compresses the spring, the cam contour is designed so that the moment arm of the cam increases monotonically with the rocker-arm angle, thereby progressively increasing the load torque on the spring. Specifically, the rocker-arm angle is denoted by θ_r, and the distance between the center of the cam follower and the cam rotation center is set to its minimum value l_{cmin} at $\theta_r = 0°$ (Fig. 2). In this configuration, the distance d shown in Fig. 2 is zero. Furthermore, by defining the contour under a constant pressure angle, a characteristic is intentionally imparted such that d increases rapidly and nonlinearly as θ_r increases. To minimize energy loss due to rolling friction, the contour is designed so that the pressure angle at the contact between the cam and the cam follower remains at 90°. Maintaining the pressure angle at 90° cancels the radial force acting on the rocker arm and thereby reduces energy loss due to rolling friction and related effects [2].

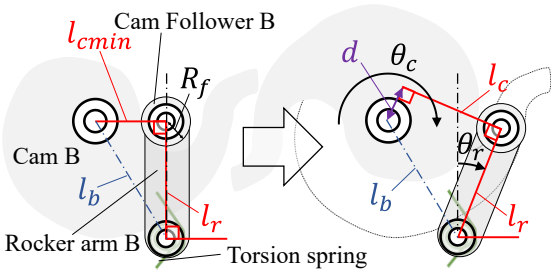

Fig. 2 Output cam model

The relationship between the torque T_c acting on the cam and the torque T_r acting on the moment arm can be obtained from the static force balance using the moment-arm lengths d and l_r, and is given by Eq. (1).

$$\frac{T_c}{d} = \frac{T_r}{l_r} \tag{1}$$

From Eq. (1), the cam torque T_c can be expressed as Eq. (2), where G denotes the reduction ratio when the rotation of the moment arm is regarded as the input and the rotation of the cam as the output.

$$T_c = \frac{d}{l_r} T_r = G T_r \tag{2}$$

From the geometric relationship involving the minimum distance l_{cmin} from the cam rotation center to the line normal to the rocker arm, l_r, and θ_r, the cam moment arm d is given by Eq. (3).

$$d = l_r(1 - cos\theta_r) + l_{cmin} sin\theta_r \tag{3}$$

Similarly, the distance lc from the cam rotation center to the line normal to the rocker arm is expressed as Eq. (4).

$$l_c = l_r sin\theta_r + l_{cmin} cos\theta_r \tag{4}$$

Substituting Eq. (4) into Eq. (2) yields the reduction ratio G as Eq. (5).

$$G = 1 - cos\theta_r + \frac{l_{cmin}}{l_r} sin\theta_r \tag{5}$$

The cam rotation angle θ_c is related to the rotation angle θ_r of the moment arm through the reduction ratio G as Eq. (6).

$$\theta_c = \frac{1}{G} \theta_r \tag{6}$$

The relationship between the cam angle θ_c and the angle of rocker arm A, θ_r is shown in Fig. 3, and the parameters used are listed in Table 2. As shown in Fig. 3, θ_r increases nonlinearly as θ_c increases, and its rate of increase gradually becomes larger. This implies that the reduction

ratio G gradually decreases with increasing θ_c. The coordinates of the cam contour corresponding to a given rocker-arm rotation angle θ_r are obtained from the geometric relations given by Eq. (7) and Eq. (8).

$$x = dcos\left(\frac{\pi}{2} - \theta_r + \theta_c\right) + (l_c - R_f)cos\,(-\theta_r + \theta_c) \qquad (7)$$

$$y = dsin\left(\frac{\pi}{2} - \theta_r + \theta_c\right) + (l_c - R_f)\,sin(-\theta_r + \theta_c) \qquad (8)$$

Using Eq. (7) and Eq. (8) together with the design parameters listed in Table 2, the resulting cam profile is plotted in Fig. 4.

Table 2 Design parameters

k	Spring constant	10Nm/rad
R_{cf}	Cam-follower radius	0.005m
$l_{c,min}$	Minimum length of l_c	0.01m
l_r	Rocker arm A length	0.05m
l_p	Pulley distance	0.12m
$\theta_{r,max}$	Maximum angle of θ_r	45°
$\theta_{r,min}$	Minimum angle of θ_r	5°
$\theta_{r,ini}$	Initial angle of θ_r	12.22°
$\theta_{sp,ini}$	Initial angle of θ_{sp}	35.84°
$\Delta\theta_{sp,max}$	Maximum spring-compression angle	35.84°
I_r	Rocker-arm A inertia	3.37×10^{-7}kgm^2
I_c	Cam inertia	3.90×10^{-8}kgm^2
I_o	Output-link inertia	5.00×10^{-7}kgm^2

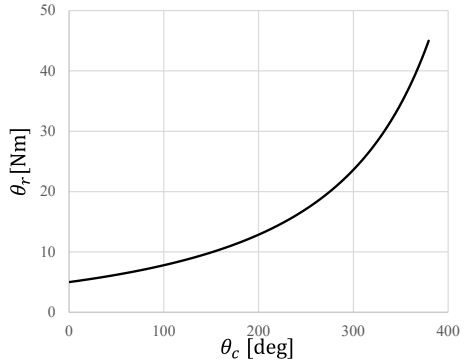

Fig. 3 Relationship between cam angle θ_c and the angle of rocker arm A, θ_r

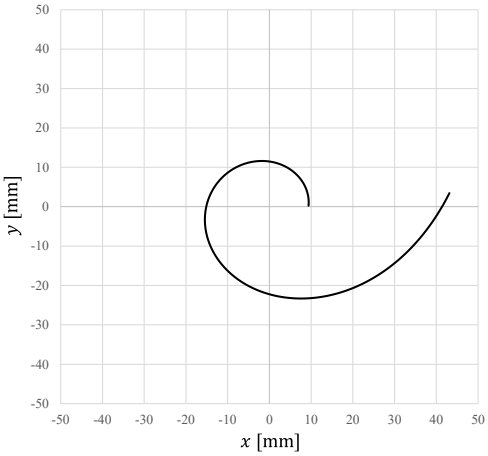

Fig. 4 Designed cam shape

Based on the designed cam, the angular velocity of the output link during rapid motion is derived using the law of conservation of energy. Immediately after the leading spring is released at the start of the rapid motion, the maximum compression angle of the remaining output-driving spring is denoted by $\Delta\theta_{sp,max}$. The moments of inertia of the rocker arm, the cam, and the output link are denoted by I_r, I_c, and I_o, respectively. Assuming no energy loss, the relationship between the potential energy stored in the two springs and the kinetic energy of each mechanical element is described by the conservation of energy, as expressed in Eq. (9).

$$\frac{1}{2}k\Delta\theta_{sp,max}{}^2 = \frac{1}{2}\left[I_r(G_1{}^2 + G_2{}^2) + 2I_c + I_o\right]\dot{\theta_o}{}^2 + \frac{1}{2}k(\Delta\theta_{r,1}{}^2 + \Delta\theta_{r,2}{}^2) \qquad (9)$$

The left-hand side of Eq. (9) represents the potential energy stored in the output-driving spring. The first term on the right-hand side represents the kinetic energy of the rocker arm, the cam, and the output link. Because these mechanical elements are subject to the deceleration (speed-reduction) effect of the cam, this term includes the reduction ratios G_1 and G_2. Here, G_1 denotes the reduction ratio of the cam corresponding to the driving spring, and G_2 denotes the reduction ratio of the cam corresponding to the reloading spring. The second term on the right-hand side represents the sum of the residual potential energy remaining on the driving-spring side and the potential energy passively reloaded on the opposite side when the spring is mechanically re-engaged. The quantities $\Delta\theta_{r,1}$ and $\Delta\theta_{r,2}$ represent the twisting-angle variations of the spring on the driving-spring side and the reloading side, respectively. Solving Eq. (9) for $\dot{\theta_o}$ yields the magnitude of the angular velocity of the output link, as expressed in Eq. (10):

$$|\dot{\theta_o}| = \sqrt{\frac{k\left(\Delta\theta_{sp,max}{}^2 - \Delta\theta_{r,1}{}^2 - \Delta\theta_{r,2}{}^2\right)}{I_r(G_1^2 + G_2^2) + 2I_c + I_o}} \qquad (10)$$

4. Analysis

4.1. Overview

To verify the effectiveness of the output cam designed in Section 3, motion simulations of the variable-stiffness and rapid-motion modes were performed using SolidWorks Motion. Fig. 5 shows a three-dimensional model of the mechanism used in these simulations. The model includes an output link, two output cams, two rocker arms for the output cams, two rocker arms for spring compression, two torsion springs, and a base. The pulleys attached to the two cams and the output link are connected by a virtual timing belt, and the transmission ratio is set to 1:1. The cam follower attached to rocker arm B is constrained to remain in contact with the contour of the output cam. A virtual torsion spring is placed between each output-cam rocker arm and its corresponding spring-compression rocker arm. The output cams, output-cam rocker arms, fixed link, and torsion springs were designed based on the design parameters listed in Table 2. The remaining parameters are also summarized in Table 2. In the present study, the torsional spring constant was set to k =10 Nm/rad as a representative assumed value for investigating the fundamental behavior of the proposed mechanism. As indicated by Eq. (10), $\dot{\theta_o}$ is proportional to k . Therefore, the value of k affects the magnitude of the angular velocity, while the qualitative tendency with respect to θ_o is preserved. This simulation neglected the effects of gravity, friction, spring damping, the mass of the timing belt, and the mass of rocker arm B. In addition, contact between mechanical elements other than the adjacent elements constrained by coincident mates was ignored, allowing them to pass through each other.

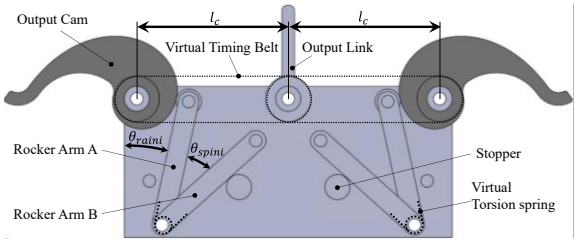

Fig. 5 Simulation model

4.2. Variable-stiffness simulation

In this simulation, the preset (preload) of the two torsion springs was varied to examine whether the output torque changes with the preset amount when a load torque is applied to the output link. The spring preset was defined by setting the rotation angle of the spring-compression rocker arm to three conditions: 0°, 10°, and 20°. The simulation procedure is as follows.

1 The spring-compression rocker arms are actively rotated to change the compression of the torsion springs, and their postures are then held.

2 The output link is actively rotated 90° counterclockwise and then stopped.

3 The procedure returns to step 1, and the compression of the springs is changed.

The simulation result for the case of a spring preset angle of 20° is shown in Fig. 6. As the output link rotates counterclockwise, the right cam rotates the corresponding rocker arm clockwise, thereby decreasing the angle between the output-cam rocker arm and the spring-compression rocker arm and compressing the virtual torsion spring. During this motion, it was observed that the cam moment arm gradually increases.

Meanwhile, the left cam also rotates clockwise owing to the belt transmission, and the reaction force of the preset spring assists the applied load torque, increasing the angle between rocker arms A and B. The simulation results are summarized in Fig. 7. As the spring preset increases, the slope of the torque curve becomes steeper, confirming that the joint stiffness changes with the spring preset.

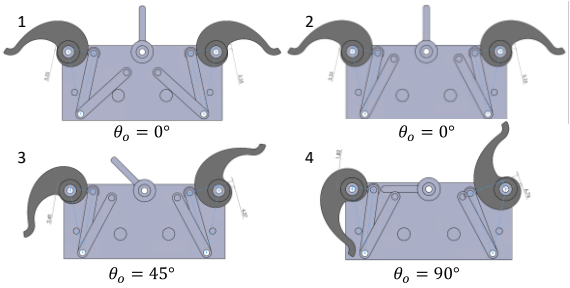

Fig. 6 Simulation of variable-stiffness behavior

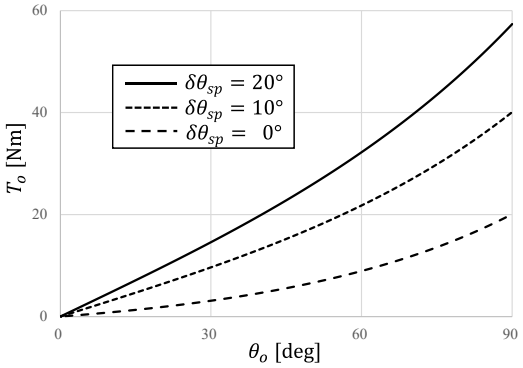

Fig. 7 Relationship between rotational angle of output link and disturbance torque

4.3. Rapid-motion simulation

In this simulation, we examined whether high-speed rotation of the output link can be achieved by instantaneously releasing one of the two compressed springs. In addition, the validity of Eq. (10), which represents the rapid-motion model developed in Section 3, was evaluated. The simulation procedure is as follows.

1. Two rocker arms A are rotated to compress the two torsion springs until the spring compression angle reaches $\theta_{sp,max}$.

2. The posture constraint of the right spring-compression rocker arm is released (its holding torque is set to zero).

The simulated motion is illustrated in Fig. 8. Immediately after the posture constraint is released in step 2, the right spring-compression rocker arm rotates clockwise under the force stored in the spring and stops when it contacts the stopper. Subsequently, the internal force balance of the mechanism is disturbed, and the torque stored in the left torsion spring is transmitted via the left output-cam rocker arm to the left cam, the central output link, the right cam, and finally the right output-cam rocker arm. These components then rotate clockwise in sequence.

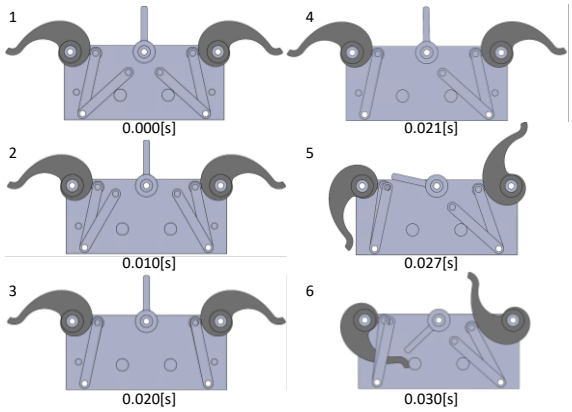

Fig. 8 Simulation of rapid motion behavior

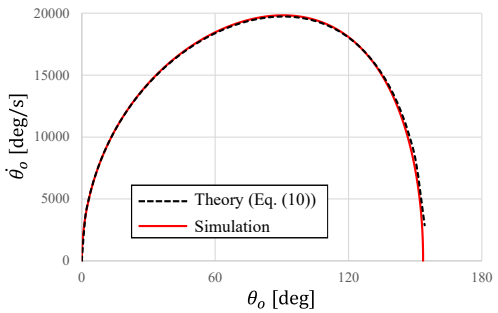

Fig. 9 Relationship between output angle θ_o and output angular velocity $\dot{\theta_o}$

Fig. 9 shows the angular velocity of the output link obtained from this simulation together with the angular velocity calculated from Eq. (10). The peak angular velocity reaches approximately 20,000 deg/s, confirming that high-speed rotation is achieved. Furthermore, the results obtained by SolidWorks Motion are in good agreement with those of the mathematical model, thereby validating the proposed analytical model. The angular velocity increases from 0° to 90° and then decreases from 90° to 180°. This behavior is due to the right cam recompressing the spring during the motion, resulting in an increased load.

5. Conclusion

This paper presented the structure of a novel rotary actuator, methods for realizing its functions, the design methodology of the output cam, an analysis of the angular velocity during rapid motion, and simulation results obtained using SolidWorks Motion. For the design of the output cam, we proposed a method for designing a cam whose reduction ratio gradually decreases, and analytical results confirmed that a characteristic in which the joint torque increases with the displacement required for variable stiffness can be realized theoretically. Furthermore, a method for achieving rapid motion using a cam designed primarily for variable stiffness was presented, and an angular-velocity model for this motion was derived. The mathematical model showed good agreement with the simulation results, thereby validating the theoretical model. The derived equation can be applied to the analysis of angular-velocity control during rapid motion and to the optimization of design parameters. In addition, the rapid-motion simulation demonstrated a maximum angular velocity of approximately 20,000 deg/s, indicating that ultrahigh-speed rotation can be achieved in theory. Future work will include detailed analysis of the variable-stiffness characteristics and experimental validation using a prototype, including comparison of the experimental results with the theoretical and simulation results. In addition, the application of the proposed actuator to a mobile robot that uses a roller-driven spherical body as its driving mechanism, as well as the analysis of its locomotion kinematics, will be investigated.

References

1. OECD, OECD Employment Outlook 2025: Can We Get Through the Demographic Crunch?, OECD Publishing, Paris, 2025.
2. OECD, The Future of Rural Manufacturing, OECD Publishing, Paris, 2023.
3. IDTechEx, The Rise of Collaborative Robots: Technical and Commercial Insights, IDTechEx Research Article, Jul. 1, 2025.
4. J.-S. Koh, S.-P. Jung, R. J. Wood, and K.-J. Cho, A jumping robotic insect based on a torque reversal catapult mechanism, in Proc. IEEE/RSJ Int. Conf. Intell. Robots Syst., Tokyo, Japan, 2013, pp. 3796–3801.
5. M. Plooij, M. Wisse and H. Vallery, Reducing the energy consumption of robots using the bidirectional clutched parallel elastic actuator, IEEE Transactions on Robotics, 32(6), 2016, pp. 1512–1523.
6. Jafari, A., Tsagarakis, N. G., Sardellitti, I., and Caldwell, D. G. A new actuator with adjustable stiffness based on a variable ratio lever mechanism. IEEE/ASME Transactions on Mechatronics 19(1), 2012, pp. 55-63.
7. Toubar, H., Awad, M. I., Boushaki, M. N., Niu, Z., Khalaf, K., and Hussain, I. Design, modeling, and control of a series elastic actuator with discretely adjustable stiffness (seadas). Mechatronics 86, 2022, 102863.
8. Sariyildiz, E., Mutlu, R., Roberts, J., Kuo, C. H., and Ugurlu, B. Design and control of a novel variable stiffness series elastic actuator. IEEE/ASME transactions on mechatronics 28(3), 2023, pp. 1534-1545.
9. H. Tomori, S. Nagai, T. Majima, and T. Nakamura, Variable impedance control with variable viscoelasticity

joint manipulator for instantaneous force, Transactions of the Society of Instrument and Control Engineers 51(6), Jun. 2015, pp. 380-389.
10. Krimsky, E., and Collins, S. H. Elastic energy-recycling actuators for efficient robots. Science Robotics, 9(88), 2024, eadj7246.
11. K. Suzuki, Y. Nishida, T. Sonoda and K. Ishii. A new rotary actuator capable of rapid motion using an antagonistic cam mechanism. Journal of Advances in Artificial Life Robotics 1(3); December (2020), pp. 144–152.
12. K. Suzuki, Y. Nishida and K. Ishii, Realizing Variable Stiffness through Structures Designed for Quick Motion. Journal of Advances in Artificial Life Robotics 4(3); June (2025), pp. 122–127.
13. K. Suzuki, Y. Nishida, K. Kimura and K. Ishii, Development of a Rotary Actuator Capable of Multidirectional Rapid Motion and Variable Stiffness, Proceedings of The 2025 International Conference on Artificial Life and Robotics (ICAROB2025), Feb13-16, J:COM Horuto Hall, Oita, Japan, pp. 369-373.

Authors Introduction

Dr. Katsuaki Suzuki

He is a Researcher at the Kumamoto Industrial Research Institute, Japan. He received his Ph.D. degree from the Kyushu Institute of Technology in 2021. His research interests include joint mechanisms and their applications.

Dr. Yuya Nishida

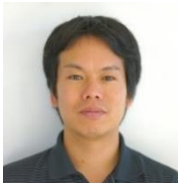

He is an Associate Professor at the Graduate School of Life Science and System Engineering, Kyushu Institute of Technology, Japan. His research interests include filed robotics, its application, and data processing.

Dr. Kenji Kimura

He is an Associate Professor at the Department of Control Engineering, National Institute of Technology, Matsue College, and a Visiting Associate Professor at Chuo University. He received his ME (mathematics) from Kyushu University in 2002 and his PhD (engineering) from the Kyushu Institute of Technology in 2020. His research interests are spherical mobile robots.

Prof. Kazuo Ishii

He received his Ph.D. degrees from Tokyo University, Japan, in 1996. In 2011, he joined Kyushu Institute of Technology, where he is currently a Professor of the Department of Human Intelligence Systems.

His research interests include Underwater Robot, Neural Network and Neural Network.